INTERNATIONAL JOURNAL OF PRECISION ENGINEERING AND MANUFACTURING Vol. 16, No. 7, pp. 1631-1637 JUNE 2015 / 1631
DOI: 10.1007/s12541-015-0214-y ISSN 2234-7593 (Print) / ISSN 2005-4602 (Online)

Motion Control of Bicycle-Riding Exoskeleton Robot with Interactive Force Analysis

Geun Sub Heo[1], Sang-Ryong Lee[1], Moon Kyu Kwak[1], Cheol Woo Park[1], Gyuman Kim[1], and Choon-Young Lee[1,#]

1 School of Mechanical Engineering, Kyungpook National University, 80 Daehak-ro, Buk-gu, Daegu, 702-701, South Korea
Corresponding Author / E-mail: cylee@knu.ac.kr, TEL: +82-53-950-7541, FAX: +82-53-950-6550

KEYWORDS: Bio-inspired control, Exoskeleton robot, Human-robot Interaction, Force interaction

Exoskeleton robots are used to augment human power to perform difficult tasks. These robots can generate eternal load on human muscles as training devices. In this paper, a lower-limb training device using exoskeleton is developed for muscle power augmentation during cyclic motion. A control system determines augmenting power on the human leg during pedaling motion based on the calculation of muscle activity timing. The resulting power of the exoskeleton assists cycling motion as a rehabilitation system or applies mechanical load on the leg muscles as a training system. Measurement of interaction force by the load cell on each pedal determines admittance control signal. Experiments to assist bicycle riding motion using the developed exoskeleton were conducted. From the interaction force analysis, the sources of errors in the motion control are found, and the application-specific problems are discussed. Given that the exoskeleton robot can control hip and knee joint independently, the proposed system can be extended for assisting various motions in daily life, including walking rehabilitation.

Manuscript received: July 14, 2014 / Revised: December 5, 2014 / Accepted: January 13, 2015

NOMENCLATURE

L_i = Length of *i*-th link
l_i = Distance to center of gravity from the *i*-th frame origin
θ_{0i} = Direction to center of gravity from the *i*-th frame origin
m_i = mass of *i*-th link
I_{izz} = Moment of inertia of *i*-th link
$\theta_{i,j}$ = sum of two angles, $\theta_i + \theta_j$

1. Introduction

Human power augmentation by robotic exoskeleton enables normal humans to manipulate objects that are out of range. In the past two decades, researchers have focused on upper limb exoskeleton for heavy industry workers in moving objects or tools to reduce load. Recently, lower limb exoskeleton robots for soldiers and disabled people have attracted interest for assistance and for training devices.[1]

Pratt et al.[2] suggested that the key functions of exoskeleton robots for humans are performance enhancement, low impedance, natural interface, life improvement, as well as comfort and safety. RoboKnee was designed to carry heavy load of 60 kg backpack without getting tired. However, no quantitative evaluation of the exoskeleton system was conducted in terms of its enhancing effect. EMG signals are shown to control the Hybrid Assistive Limb (HAL) as a device assisting in swing motion of operator's leg.[3] The device developed by Cyberdyne, Inc. obtained CE Marking (CE 0197) as a medical device in EU.[4] Exoskeleton robot with multi-degrees of freedom is used to train post-stroke patients by allowing adaptation of human subject's gait phase with intelligent control strategies.[5] The coordinated movement of exoskeleton with the user's motion is shown by the experiment through adapting gait cycles. Although encouraging remarks are given by the patients, a rigorous quantitative evaluation on the performance in rehabilitation aspect or assistive method is needed. Analytical model of the knee is suggested to estimate internal forces by muscles during exercise for the eight groups.[6] Optimization technique is used to estimate muscle forces and showed that muscle force model is only valid in quasi-static (low speed) exercise. Virtual modification of the mechanical impedance of the human limbs is suggested to improve kinematic response of the limb.[7] The state of the art clinical motion analysis is reviewed for the estimation of muscle forces from computational model.[8]

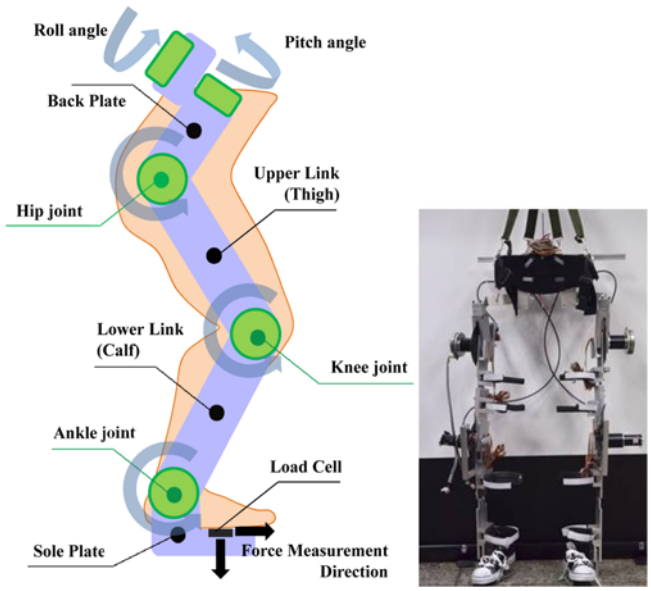

Fig. 1 Mechanical design of exoskeleton robot and the developed system

In clinical studies, bicycle riding showed promising results for treating patients with Parkinson's disease.[9] Dynamic model of the bicycle robot using Kane's method is examined through numerical simulation to show the efficiency of the model.[10] Robotic rig for testing bicycle transmission and bicycle ergometer with a tilting seat, backboard, a split crank, and two belt-driven motors are developed to provide both power to assist the user and resistance loads for training.[11,12]

In this study, an exoskeleton robot is developed to train or assist leg muscles and evaluate the capability to compensate loading by analyzing load cell force data. Motion capture data of human cycling is used to develop reference trajectories of exoskeleton robot. Load cell sensors located on the sole of robotic suit and on the pedal of the bicycle are used to measure interaction force. A comparison is conducted between exercises with augmented power from exoskeleton and the exercises without additional augmentation during the bicycle riding. Experimental results with interaction force analysis are presented and discussed; conclusion and future research directions are provided.

2. Design of Exoskeleton Robot for Bicycle Riding

The exoskeleton robot for bicycle riding is designed to assist human leg motion in daily life. The hip joints and knee joint are actuated by brushless DC motor with driver. The hip joints are configured as 3 degrees of freedom with passively rotating back plates to follow body rotation. One actuated joint gives hip flexion and extension of thigh segment. The knee joint is designed to allow single rotation of knee flexion. The ankle joint is designed as single passive joint used to rotate freely according to the resulting motion of the foot. As reported in Ref. 20, the percentage of mechanical work in ankle joint during bicycle riding is below 10% of the total work.[20] Therefore, in the present study, the actuation of ankle joint is omitted for the user to adjust own motion of ankle during the bicycle ride.

Table 1 Requirement of joints

Joint Motion	Range of Motion [°]	Angular Velocity [°/s]	Maximum Torque [Nm]
Hip Flexion	90	40	10
Hip Extension	25	40	10
Knee Flexion	90	120	20
Ankle Flexion	20	150	20
Ankle Extension	15	150	20

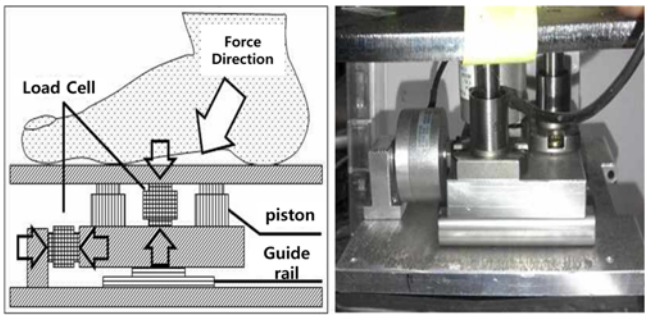

Fig. 2 Pedal subsystem to measure interactive forces

Table 2 Kinematic and dynamic parameters

Property	Notation	Value
Distance to COG from origin	l_1 [m]	0.209
	l_2 [m]	0.105
Angles to COG from origin	θ_{01} [°]	3.205
	θ_{02} [°]	11.976
Length	L_1 [m]	0.377
	L_2 [m]	0.403
	L_3 [m]	0.103
Mass	m_1 [kg]	3.589
	m_2 [kg]	1.93
Moment of Inertia	I_{1zz} [kg·m^2]	0.109
	I_{2zz} [kg·m^2]	0.052

2.1 Mechanical design

Fig. 1 shows the outline of mechanical structure of the developed exoskeleton robot. The range of motion for each joint is chosen in accordance with the general human joint angles in daily life. For the safety of the user, the researchers applied constraints on the range of mechanical motion to avoid rotation of the robot in extreme angles. Table 1 lists the requirement of leg joints for a range of motion.[13] The EC 90 flat 90W Maxon motor with reduction gear with a ratio of 81:1 is used for actuating the hip joint. The EC 40 flat 120W brushless DC motor with planetary gear and reduction ratio of 81:1 is implemented to rotate the knee joint. The motor drivers are 4-quadrant digital controller for brushless EC motors (DEC 70/10 model).

Fig. 2 shows the pedal subsystem measuring interactive forces by foot pressure on the bicycle pedal resulting to torques on the crank. Guide rail and pistons are designed to apply forces into two load cells through the structure. Miniature load cell such as the Ktoyo Model 247ST with a rated capacity of 50 kg is used to measure tension and compression forces.

Listed in Table 2 are the derived dynamic parameters of the exoskeleton robot using 3D-CAD model in CATIA V5.18. The

parameters for ankle joint are omitted as the joint is passive. Each leg is modeled as two degrees of freedom planar manipulator, which corresponds to hip and knee joints. The kinematics and dynamic equations are discussed in Section 3.

2.2 Embedded control system

Roll and pitch angles of back plate in Fig. 1 are measured by two-axis gyro sensor such as the Attitude Reference System (ARS). The sensor implemented Kalman Filters to generate angle data with 100 Hz through UART interface. The measurement of roll and pitch angles ranges from -60° to +60°. In addition to incremental encoder, Autonics E40 Series with 360 pulse/revolution, the researchers interfaced magnetic type absolute encoder to measure joint angles. RMB20SC, absolute binary synchro-serial interface (SSI) type, is connected to the main CPU. The pulses with 4096 counts/rev. correspond to resolution of 0.09° to determine joint angles.

Fig. 3 shows the signal flow of the whole hardware control system. Distributed control architecture is implemented to control the motion of exoskeleton robot. Each joint actuator is controlled by a microcontroller that receives reference trajectory command from the main CPU. The main controller is ARM 32-bit Cortex™, the M3 CPU (STM32F Series), which calculates command signals for each joint based on various states such as posture, joint angles, and foot force among others.[14] The main controller is connected directly to the absolute encoders, feedback signal line of each motor driver, and a number of stand-alone microcontrollers. The sub-controllers for motor control, force measurement, and body posture measurement are AVR ATmega 8-bit microcontrollers (ATmega128). Each processor is used for AD-conversion of force signals to receive roll and pitch angle through UART communication channel, as well as to generate PWM command signal as stand-alone processors.

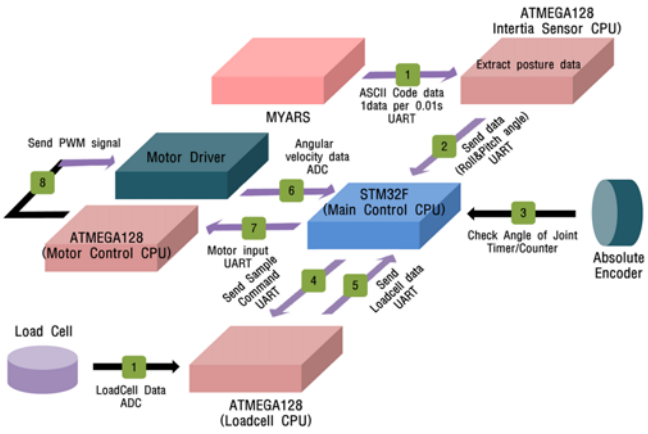

Fig. 3 Embedded control system architecture: (1) measurement of load cells, roll and pitch angles, (2) sending attitude information (roll and pitch angle to main CPU), (3) checking joint angles of leg segments, (4) request of load cell data, (5) sending load cell data to main CPU, (6) sending angular velocities of each joint to main CPU, (7) command signal of motor operation, (8) and command signal to motor driver for generating PWM pulse

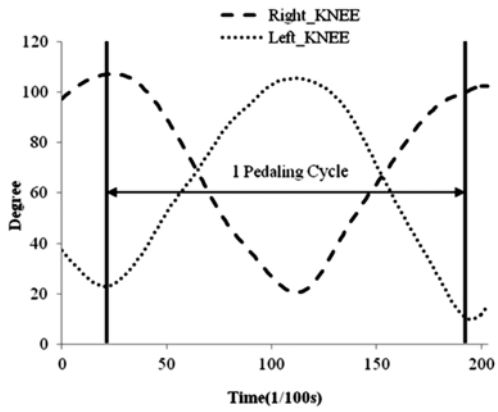

Fig. 4 Knee angles for right and left leg during cycling motion

3. Motion Control Algorithm

In this section, constraints in the cycling motion are discussed and the kinematic and dynamic equations are derived with interaction force analysis. Based on the mathematical results, the robot motion control algorithm is implemented.

3.1 Cycling motion analysis

To analyze human cycling motion, optical motion capture system is used to obtain joint angles during the bicycle ride. Optical motion capture system is able to construct human body model based on joint angles during pedaling. The phase difference between the left and the right knees during pedaling motion is shown in Fig. 4. This difference is the constraint of bicycle riding assuming that two feet are always positioned on the pedals.

$$\theta_{Lc}(t) - \theta_{Rc}(t) = \pi \tag{1}$$

where θ_{Lc}, θ_{Rc} are the angles of crank for the left and right feet in radian measure.

Using the coordinate system in Fig. 5, forward kinematics is easily derived. The positions of reference pedal for each leg is represented as follows:

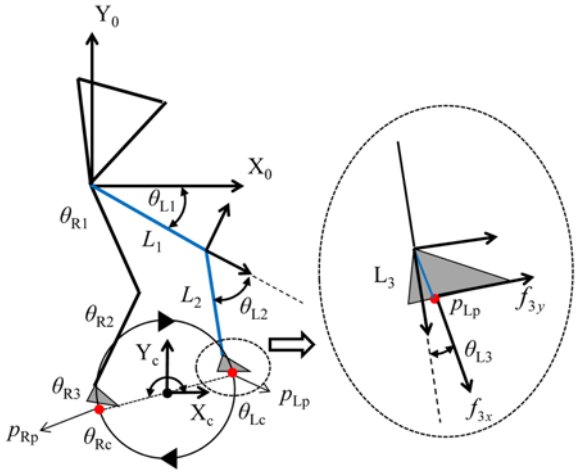

Fig. 5 Kinematic relation of the exoskeleton robot with crank coordinate system

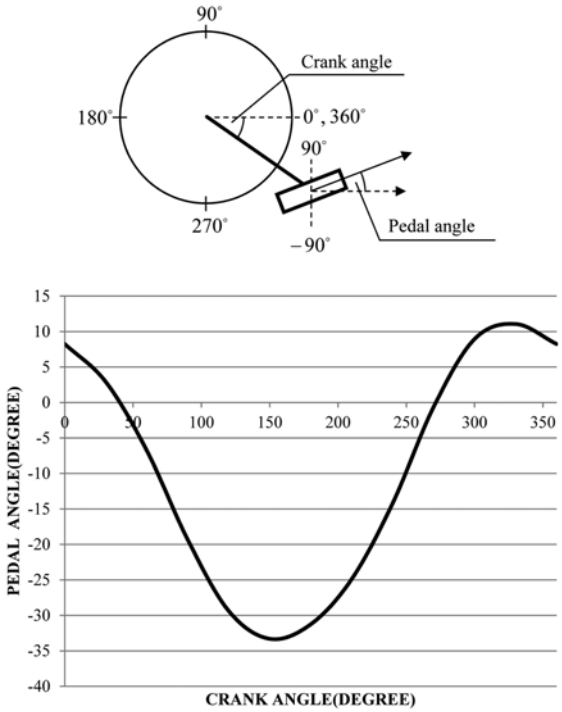

Fig. 6 Ankle motion of pedaling by an expert cyclist with respect to crank angle

$$ {}^{0}p_{Rp} = \begin{bmatrix} L_1\cos(\theta_{R1}) + L_2\cos(\theta_{R1}+\theta_{R2}) + L_3\cos(\theta_{R1}+\theta_{R2}+\theta_{R3}) \\ L_1\sin(\theta_{R1}) + L_2\sin(\theta_{R1}+\theta_{R2}) + L_3\sin(\theta_{R1}+\theta_{R2}+\theta_{R3}) \\ 0 \end{bmatrix} \quad (2) $$

$$ {}^{0}p_{Lp} = \begin{bmatrix} L_1\cos(\theta_{L1}) + L_2\cos(\theta_{L1}+\theta_{L2}) + L_3\cos(\theta_{L1}+\theta_{L2}+\theta_{L3}) \\ L_1\sin(\theta_{L1}) + L_2\sin(\theta_{L1}+\theta_{L2}) + L_3\sin(\theta_{L1}+\theta_{L2}+\theta_{L3}) \\ 0 \end{bmatrix} \quad (3) $$

where θ_{Li}, θ_{Ri}, $i = 1, 2, 3$ are joint angles (hip, knee, and ankle) of exoskeleton for the left and right legs.

In this study, the researchers aim to control exoskeleton in assisting cycling motion, therefore, reference trajectory of pedal position when appropriate pedaling motion is generated. Given the position of the pedal except its direction, infinitely many inverse kinematics solutions are available for the kinematics of Eqs. (2) and (3), thus, the system is redundant. Given the passive joint of the exoskeleton at the ankle mechanism, the possible angle at the ankle joint is assumed to be adjusted by the user. To solve the inverse kinematics problem, the inherent redundancy is resolved by using the motion of an expert cyclist. Expert cyclist shows the tendency of pedal angle with respect to the crank angle as shown in Fig. 6.

The pedal angle is a function of crank angle, thus, we can assume the relations of $\theta_{Lp} = f(\theta_{Lc})$, $\theta_{Rp} = f(\theta_{Rc})$. For the left leg, foot orientation is related to the pedal angle given by,

$$ \theta_{L1} + \theta_{L2} + \theta_{L3} = \theta_{Lp} - \pi/2 \quad (4) $$

$$ {}^{0}p_{Lp} = \begin{bmatrix} L_1\cos(\theta_{L1}) + L_2\cos(\theta_{L1}+\theta_{L2}) + L_3\cos(\theta_{Lp}) \\ L_1\sin(\theta_{L1}) + L_2\sin(\theta_{L1}+\theta_{L2}) + L_3\sin(\theta_{Lp}) \\ 0 \end{bmatrix} = \begin{bmatrix} x \\ y \\ 0 \end{bmatrix} \quad (5) $$

Let

$$ \cos(\theta_{L2}) = \frac{(x - L_3\sin(\theta_{Lp}))^2 + (y + L_3\cos(\theta_{Lp}))^2 - L_1^2 - L_2^2}{2L_1L_2} $$

And

$$ \sin(\theta_{L2}) = -\sqrt{1 - \cos^2(\theta_{L2})} \le 0 $$

then, the following inverse kinematics solution is obtained.

$$ \theta_{L2} = \operatorname{atan2}(\sin(\theta_{L2}), \cos(\theta_{L2})) \quad (6) $$

$$ \begin{aligned} \theta_{L1} = {} & \operatorname{atan}(y + L_3\cos(\theta_{Lp}), x - L_3\sin(\theta_{Lp})) \\ & - \operatorname{atan}(L_2\sin(\theta_{L2}), L_1 + L_2\cos(\theta_{L2})) \end{aligned} \quad (7) $$

$$ \theta_{L3} = \theta_{Lp} - \pi/2 - \theta_{L1} - \theta_{L2} \quad (8) $$

The resulting joint angles shown in Eqs. (6) and (7) are the reference joint trajectories for the exoskeleton. The right side of Eq. (4) is the normal direction of foot to the ground side.

Iterative approach may be used by searching a local solution through pseudo-inverse of Jacobian matrix and projecting the homogeneous solution on the null space of the Jacobian.[15]

3.2 Interactive force analysis

Interaction between exoskeleton and human limb results in the modification of impedance properties for the coupled system. The control of impedance imposes margin on the tracking error. The impedance describes a force or velocity relation of the bicycle pedal[16]

$$ \frac{f_p(s)}{sx(s)} = Z(s) = M_i s + B_i + \frac{D_i}{s} \quad (9) $$

where f_p represents the force applied on the pedal, and x is the displacement at the contact point. The term Z is the impedance between the robotic foot and the bicycle pedal, M_i, B_i, and D_i are parameters such that the closed-loop system behaves as a desired impedance model

$$ M_i\ddot{x}_e + B_i\dot{x}_e + D_i x_e = f_p $$

where $x_e = x_d - x$ is the position error.

Muscle tension (joint moments) is related to the measured pedal force from which the leg's weight and inertia are subtracted.[17] The concept makes it possible to relate the measurement of forces directly on the shoe plate by load cells to the muscle activity. The admittance control using the interaction force, f_d and design parameters of M_a, B_a, and D_a are characterized by

$$ \frac{sx(s)}{f_d(x)} = R(s) = M_a s + B_a + \frac{D_a}{s} \quad (10) $$

PID admittance control algorithm based on Eq. (10) is known better than impedance filter when position error exists.[18]

3.3 Motion control of exoskeleton

Using the iterative Newton-Euler dynamic formulation, the following dynamic equations are derived for the exoskeleton robot.

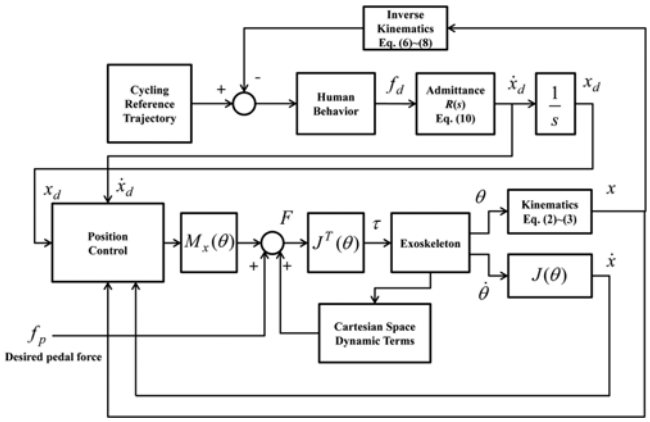

Fig. 7 Admittance control architecture of exoskeleton robot

$$\begin{aligned}\tau_1 &= [m_1 l_1^2 + m_2 l_2^2 + m_2 L_1^2 + 2m_2 l_2 L_1 \cos(\theta_{2,02})]\ddot{\theta}_1 \\ &+ (I_{1zz} + I_{2zz})\ddot{\theta}_1 + [m_2 l_2^2 + m_2 l_2 L_1 \cos(\theta_{2,02}) + I_{2zz}]\ddot{\theta}_2 \\ &- 2m_2 l_2 L_1 \sin(\theta_{2,02})\dot{\theta}_1\dot{\theta}_2 - 2m_2 l_2 L_1 \sin(\theta_{2,02})\dot{\theta}_2^2 \\ &+ [m_2 l_2 \cos(\theta_{1,2,02}) + m_1 l_1 \cos(\theta_{1,01}) + m_2 L_1 \cos\theta_1]g \\ &+ [L_2 \sin\theta_3 + L_1 \sin(\theta_{2,3}))]f_x + [L_2 \cos\theta_3 + L_1 \cos(\theta_{2,3})]f_y\end{aligned} \tag{11}$$

$$\begin{aligned}\tau_2 &= [m_2 l_2^2 + m_2 l_2 L_1 \cos(\theta_{2,02}) + I_{2zz}]\ddot{\theta}_1 \\ &+ [m_2 l_2^2 + I_{2zz}]\ddot{\theta}_2 \\ &+ m_2 l_2 L_1 \sin(\theta_{2,02})\dot{\theta}_1^2 + m_2 l_2 \cos(\theta_{1,2,02})g \\ &+ L_2 \sin\theta_3 f_x + L_2 \cos\theta_3 f_y\end{aligned} \tag{12}$$

where τ_i, $\theta_i (i = 1, 2)$ indicates torque and joint angle of hip and knee link, and g is the gravitation constant. Two or more subscripts in $\theta_{i,j}$ corresponds to the sum of $\theta_i + \theta_j$. The matrix form of exoskeleton dynamics in configuration space is given by,

$$\begin{bmatrix}\tau_1 \\ \tau_2\end{bmatrix} = M(\theta)\begin{bmatrix}\ddot{\theta}_1 \\ \ddot{\theta}_2\end{bmatrix} + B(\theta)\begin{bmatrix}\dot{\theta}_1 \dot{\theta}_2\end{bmatrix} + C(\theta)\begin{bmatrix}\dot{\theta}_1^2 \\ \dot{\theta}_2^2\end{bmatrix} + G(\theta) + J^T(\theta)\begin{bmatrix}f_x \\ f_y\end{bmatrix} \tag{13}$$

where $M(\theta)$ is the mass matrix, $B(\theta)$ is the Coriolis term, $C(\theta)$ is the centrifugal term, $G(\theta)$ is the gravity term, and $J(\theta)$ is the Jacobian matrix. The term $[f_x \; f_y]^T$ is the force at the ankle corresponding to the pedal force, ${}^2_3R[f_{3x} \;\; f_{3y}]^T$.

Fig. 7 shows the overall control architecture of the exoskeleton robot using admittance model. Cycling reference trajectory is generated using expert cyclist motion. The user starts the pedaling motion, and the interaction force generates the desired motion signal to control the exoskeleton. Position control block and the rest computed torque module are used to compute the appropriate torque signal for the exoskeleton. Desired pedal force is the converted force in the ankle coordinate system.

4. Experimental Results and Discussion

We acquired joint angles by wearing the exoskeleton robotic suit in passive mode. Without power augmentation at the passive mode, the user is requested to pedal the crank with his power alone. Using the acquired data, pedal angles are modeled with respect to crank angles as shown in Fig. 6.

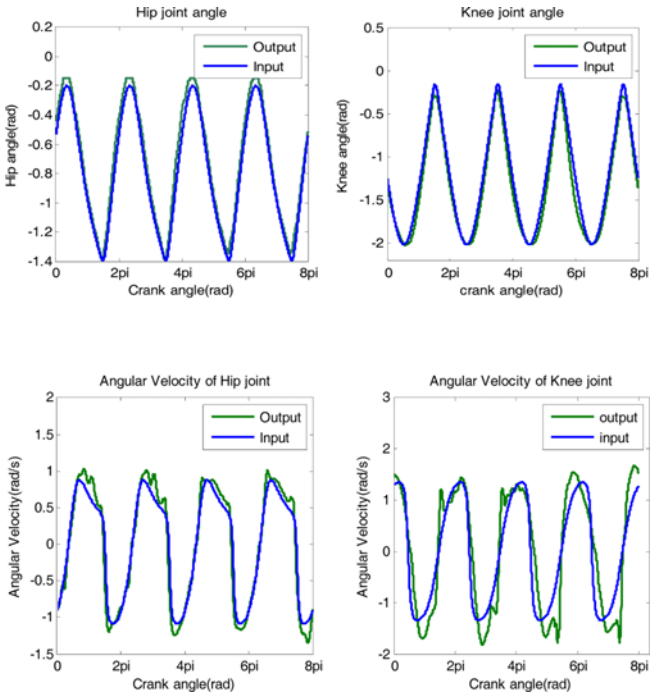

Fig. 8 Bicycle riding motion control

Fig. 8 shows the results of motion control during the pedaling motion. The joint angles at the hip and the knee are shown with respect to crank angles. Note that the graph is read in backward direction because the crank rotates clockwise, whereas the definition of crank angle is counterclockwise. By reading the graph from right to left, the phase delay of knee joint is observed to be approximately 90 degrees relative to the hip joint motion. To meet the designed admittance model, Cartesian space trajectories are generated by the user's behavior in real time. The errors of joint angles are acceptable except for the extreme condition of the maximum and minimum flexion of joints.

The tracking errors are mainly caused by the unknown disturbance in the system dynamics and dynamic coupling with the human user. Another source of error in the motion control is the passive ankle joint in the exoskeleton. The ankle joint is controlled by the user according to the interaction force and the intention of pedaling during control. If the pedaling angle and the user's ankle motion are mismatched, then the errors in the hip and knee joints follow to compensate. Although some errors are present, the assistance of exoskeleton in pedaling motion seems to be promising on the basis of the experimental results. Given that nonlinear interaction exists between the robot and the user, admittance model is very important in minimizing the interaction force or torque and in giving comfort to the user through the motion of the exoskeleton.

The comparison of forces on the pedal with and without power augmentation is shown in Fig. 9, which is the interaction force between human foot and the robotic exoskeleton (Test image is shown in Fig. 10). The force is the absolute magnitude of tension and compression components. In passive mode, the exoskeleton only moves through the human muscle power. In that case, larger forces are needed for upward

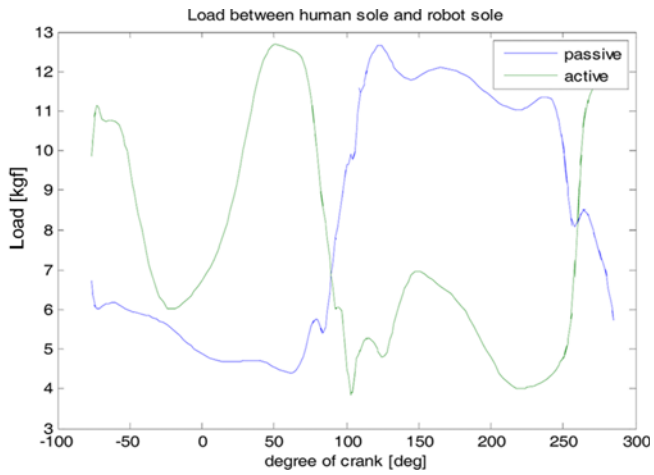

Fig. 9 Pedal force response

Fig. 10 Test image of bicycle riding

pedaling than in the downward pedaling. The exoskeleton generates driving power in active mode according to the controller output for the crank to rotate in a circular trajectory by assisting human leg motion. Given that the exoskeleton pushes the pedal downward in the first half part, larger interaction forces (tension force) are observed than those in passive mode. However, small interaction forces for active mode in the last half part appear where crank moves upward, because exoskeleton pushes human foot upward in the same direction, compared with that large forces observed in passive mode without power augmentation.

By comparing the sum of interaction forces for the interval of torque saving (90 degrees to 90 degrees) in pedaling motion for active and passive modes, the value in active mode is smaller by 72 percent than that in passive mode. Therefore, the exoskeleton can assist human pedaling motion in bicycle riding by relieving significant portion of human effort.

When a system for rehabilitation of the disabled is used, analysis on similarity of leg motion is important for the improvement of motion in the course of training. The trajectories represented on the reduced dimension characterize specific activities. Further analysis on the trajectory of the transformed space will provide useful information on the activity and the characteristic properties, such as the similarity between two limbs or between motions, can be assessed. Trajectories in high dimensional space mapped on the reduced dimension of intrinsic degrees of freedom can be classified and recognized efficiently through the process of abstraction and representation, such as locality preserving projections.[19] The motion control system will be modified using compact hall sensor array and system modification will be continued.[21]

5. Conclusions

In this paper, a new approach in applying wearable exoskeleton robot in bicycle riding is proposed. An experiment of admittance control to assist pedaling motion is conducted. From motion capture data for real human bicycle riding, the characteristic motion of bicycle pedaling and the associated joint angles have been studied. Forward and inverse kinematics for the exoskeleton leg joints is analyzed to control the wearable robot to assist human bicycle riding. The actual experimental data are discussed to emphasize the importance of ankle rotation in actual pedaling.

The interaction force and its effect on the muscle training while doing other activities other than bicycle riding will be investigated. The simplified representation of complex human motion in the reduced space will be applied to the admittance control. Development of wearable robot-based fitness system will be another area of interest.

ACKNOWLEDGEMENT

This work was supported by the National Research Foundation of Korea grant funded by Priority Research Centers Programs, NRF (2012-0005856), Basic Science Research Program, NRF (2011-0023 437), Korea-EU Researcher Exchange Program (NRF-2014K2A7A104 4147).

REFERENCES

1. Chu, A., Kazerooni, H., and Zoss, A., “On the Biomimetic Design of the Berkeley Lower Extremity Exoskeleton (BLEEX),” Proc. of the IEEE International Conference on Robotics and Automation, pp. 4345-4352, 2005.

2. Pratt, J. E., Krupp, B. T., Morse, C. J., and Collins, S. H., “The Roboknee: An Exoskeleton for Enhancing Strength and Endurance during Walking,” Proc. of IEEE International Conference on Robotics and Automation, Vol. 3, pp. 2430-2435, 2004.

3. Hayashi, T., Kawamoto, H., and Sankai, Y., “Control Method of Robot Suit HAL Working as Operator's Muscle using Biological and Dynamical Information,” Proc. of IEEE/RSJ International Conference on Intelligent Robots and Systems, pp. 3063-3068, 2005.

4. Cyberoyne, “Press Release, [News] HAL® for Labor Support (Lumbar Type) to Europe ~ the world’s first CE Marking on a wearable robot

for labor ~," http://www.cyberdyne.jp/english/company/PressReleases_detail.html?id=1810 (Accessed 20 MAY 2015)

5. Zhang, J. F., Dong, Y. M., Yang, C. J., Geng, Y., Chen, Y., and Yang, Y., "5-Link Model based Gait Trajectory Adaption Control Strategies of the Gait Rehabilitation Exoskeleton for Post-Stroke Patients," Mechatronics, Vol. 20, No. 3, pp. 368-376, 2010.
6. Zheng, N., Fleisig, G. S., Escamilla, R. F., and Barrentine, S. W., "An Analytical Model of the Knee for Estimation of Internal Forces during Exercise," Journal of Biomechanics, Vol. 31, No. 10, pp. 963-967, 1998.
7. Aguirre-Ollinger, G., Colgate, J. E., Peshkin, M. A., and Goswami, A., "Active-Impedance Control of a Lower-Limb Assistive Exoskeleton," Proc. of IEEE 10th International Conference on Rehabilitation Robotics, pp. 188-195, 2007.
8. Erdemir, A., McLean, S., Herzog, W., and Van Den Bogert, A. J., "Model-based Estimation of Muscle Forces Exerted during Movements," Clinical Biomechanics, Vol. 22, No. 2, pp. 131-154, 2007.
9. Song, C. G., Kim, J. Y., and Kim, N. G., "A New Postural Balance Control System for Rehabilitation Training based on Virtual Cycling," IEEE Transactions on Information Technology in Biomedicine, Vol. 8, No. 2, pp. 200-207, 2004.
10. Huang, Y., Wei, S., and Guo, L., "Dynamic Modeling of a Bicycle Robot with Front-Wheel Drive based on Kane's Method," Proc. of IEEE International Conference on Information and Automation (ICIA), pp. 758-764, 2010.
11. Shooter, S. B., Thorpe, J. I., Sutton, E. B., and Kobel, K., "Design of a Robotic Rig for Testing Bicycle Transmissions," Proc. of IEEE/RSJ International Conference on Intelligent Robots and Systems, Vol. 2, pp. 1838-1843, 2002.
12. Van der Loos, H., Worthen-Chaudhari, L., Schwandt, D., Bevly, D. M., and Kautz, S. A., "A Split-Crank Bicycle Ergometer uses Servomotors to Provide Programmable Pedal Forces for Studies in Human Biomechanics," IEEE Transactions on Neural Systems and Rehabilitation Engineering, Vol. 18, No. 4, pp. 445-452, 2010.
13. Anwar, T. and Jumaily, A. A., "Patient Cooperative Adaptive Controller for Lower Limb Robotic Rehabilitation Device," Proc. of IEEE International Advance Computing Conference (IACC), pp. 1469-1474, 2014.
14. STMicroelectronics, "STM32 32-bit ARM Cortex MCUs," http://www.st.com/web/en/catalog/mmc/FM141/SC1169 (Accessed 20 MAY 2015)
15. Bonnet, V., Mazza, C., Fraisse, P., and Cappozzo, A., "Real-Time Estimate of Body Kinematics during a Planar Squat Task using a Single Inertial Measurement Unit," IEEE Transactions on Biomedical Engineering, Vol. 60, No. 7, pp. 1920-1926, 2013.
16. Hogan, N., "Impedance Control: An Approach to Manipulation: Part I-Theory," Journal of Dynamic Systems, Measurement, and Control, Vol. 107, No. 1, pp. 1-7, 1985.
17. Papadopoulos, J. M., "Forces in Bicycle Pedalling, http://ruina.tam.cornell.edu/research/topics/bicycle_mechanics/forces_bicycle_pedaling.pdf (Accessed 23 FEB 2015)
18. Yu, W., Rosen, J., and Li, X., "PID Admittance Control for an Upper Limb Exoskeleton," Proc. of American Control Conference (ACC), pp. 1124-1129, 2011..
19. Lee, S. R., Heo, G. S., and Lee, C. Y., "Representation and Symbolization of Motion Captured Human Action by Locality Preserving Projections," Appplied Mathematics & Information Sciences, Vol. 8, No. 1, pp. 441-446, 2014.
20. Bini, R. R., Hume, P. A., and Kilding, A. E., "Saddle Height Effects on Pedal Forces, Joint Mechanical Work and Kinematics of Cyclists and Triathletes," European Journal of Sport Science, Vol. 14, No. 1, pp. 44-52, 2014.
21. Ahn, H. J. and Kim, K. R., "2D Hall Sensor Array for Measuring the Position of a Magnet Matrix," Int. J. Precis. Eng. Manuf.-Green Tech., Vol. 1, No. 2, pp. 125-129, 2014.